Article

Cell Reports

Formation of Chromosomal Domains by Loop Extrusion

Graphical Abstract

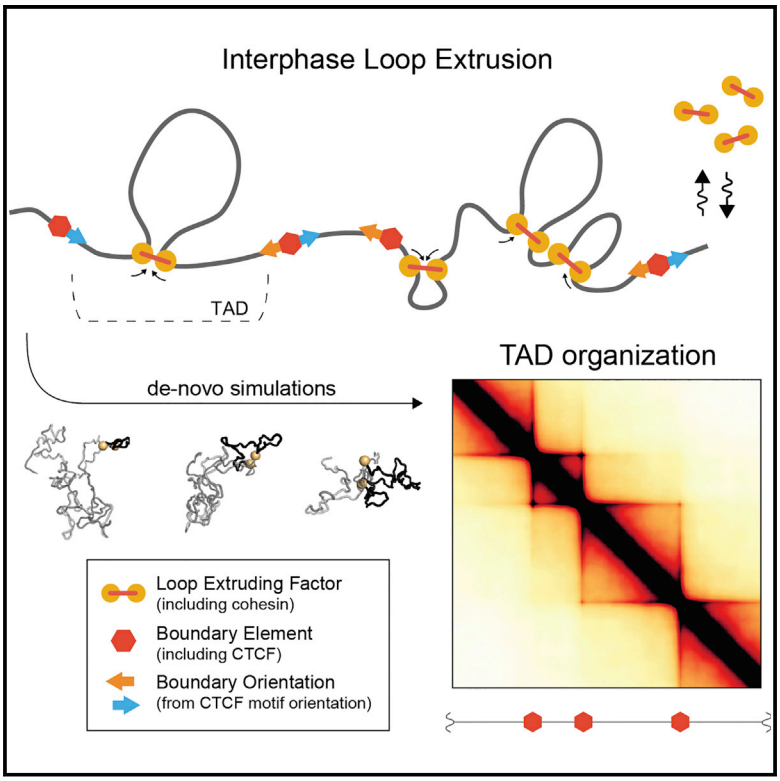

Authors

Geoffrey Fudenberg, Maxim Imakaev, Carolyn Lu, Anton Goloborodko, Nezar Abdennur, Leonid A. Mirny

Correspondence

leonid@mit.edu

In Brief

Topologically associating domains (TADs) are fundamental building blocks of human interphase chromosomes. Fudenberg et al. propose that TADs emerge as a consequence of loop extrusion limited by boundary elements. The authors use polymer simulations and genomic analyses to identify molecular roles for the architectural proteins cohesin and CTCF.

Highlights

- TADs can be formed by loop extrusion limited by boundary elements
- Polymer simulations and genomic analyses were jointly used to test this proposal
- Proposed roles of cohesin and CTCF reconcile diverse experimental observations

Fudenberg et al., 2016, Cell Reports *15*, 2038–2049
May 31, 2016
http://dx.doi.org/10.1016/j.celrep.2016.04.085

OPEN ACCESS
CellPress

Cell Reports
Article

Formation of Chromosomal Domains by Loop Extrusion

Geoffrey Fudenberg,[1,2,6] Maxim Imakaev,[3,6] Carolyn Lu,[4] Anton Goloborodko,[3] Nezar Abdennur,[5] and Leonid A. Mirny[1,2,3,*]

[1]Graduate Program in Biophysics, Harvard University, Cambridge, MA 01238, USA
[2]Institute for Medical Engineering and Science, Massachusetts Institute of Technology (MIT), Cambridge, MA 02139, USA
[3]Department of Physics, Massachusetts Institute of Technology (MIT), Cambridge, MA 02139, USA
[4]Program for Research in Mathematics, Engineering and Science for High School Students (PRIMES) and Undergraduate Research Opportunities Program (UROP), MIT, Cambridge, MA 02139, USA
[5]PhD Program in Computational and Systems Biology, MIT, Cambridge, MA 02139, USA
[6]Co-first author, listed alphabetically
*Correspondence: leonid@mit.edu
http://dx.doi.org/10.1016/j.celrep.2016.04.085

SUMMARY

Topologically associating domains (TADs) are fundamental structural and functional building blocks of human interphase chromosomes, yet the mechanisms of TAD formation remain unclear. Here, we propose that loop extrusion underlies TAD formation. In this process, *cis*-acting loop-extruding factors, likely cohesins, form progressively larger loops but stall at TAD boundaries due to interactions with boundary proteins, including CTCF. Using polymer simulations, we show that this model produces TADs and finer-scale features of Hi-C data. Each TAD emerges from multiple loops dynamically formed through extrusion, contrary to typical illustrations of single static loops. Loop extrusion both explains diverse experimental observations—including the preferential orientation of CTCF motifs, enrichments of architectural proteins at TAD boundaries, and boundary deletion experiments—and makes specific predictions for the depletion of CTCF versus cohesin. Finally, loop extrusion has potentially far-ranging consequences for processes such as enhancer-promoter interactions, orientation-specific chromosomal looping, and compaction of mitotic chromosomes.

INTRODUCTION

Interphase chromosome organization in three dimensions underlies critical cellular processes, including gene regulation via enhancer-promoter interactions. Mapping chromosomal interactions genome-wide has revealed that interphase chromosomes of higher eukaryotes are partitioned at a sub-megabase scale into a sequence of self-interacting regions, termed topologically associating domains (TADs; Dixon et al., 2012; Nora et al., 2012), or domains (Rao et al., 2014; Sexton et al., 2012). An increasing number of studies have found important functional roles for TADs in the control of gene expression and development (Andrey et al., 2013; Lupiáñez et al., 2015; Symmons et al., 2014).

TADs are contiguous regions of enriched contact frequency that appear as squares in a Hi-C map (Figure 1A), which are relatively insulated from neighboring regions. Many TADs have homogeneous interiors, while others have particularly enriched boundaries, or even more complex features. More recently, high-resolution maps revealed peaks of interactions between loci at the boundaries of TADs ("peak loci"; Rao et al., 2014). TADs differ from larger scale A/B compartments in that they do not necessarily form an alternating "checkerboard" pattern of enriched contact frequencies (Lajoie et al., 2015), and several TADs often reside within a single contiguous compartment (Gibcus and Dekker, 2013; Gorkin et al., 2014) (Supplemental Notes).

Although often illustrated as such, several lines of evidence indicate that TADs are not simply stable loops formed between pairs of boundary loci. First, only 50% of TADs have corner-peaks (Rao et al., 2014). Second, boundary loci do not appear to be in permanent contact either by fluorescence in situ hybridization (FISH) (Rao et al., 2014) or by their relative contact frequency (see Results). Third, while TADs are enriched in contact probability throughout the domain, polymer simulations show that simple loops display enrichment only at the loop bases, unless the loop is very short (Benedetti et al., 2014; Doyle et al., 2014). For these reasons, identifying mechanisms of how TADs are formed remains an important open question.

While polymer models have provided insight into multiple levels of chromosome organization (Baù et al., 2011; Lieberman-Aiden et al., 2009; Marko and Siggia, 1997; Naumova et al., 2013; Rosa and Everaers, 2008), relatively few have focused on TADs. Of those that have considered TADs, some have focused primarily on characterizing chromosome structure rather than the mechanisms of folding (Giorgetti et al., 2014; Hofmann and Heermann, 2015). Others (Barbieri et al., 2012; Jost et al., 2014) have considered models where monomers of the same type experience preferential pairwise attractions to produce TADs; such models, however, when generalized to the genome-wide scale, would require a separate factor to recognize and compact each TAD. With only several types of monomers, this would produce checkerboard patterns for each type, which is characteristic of compartments rather than

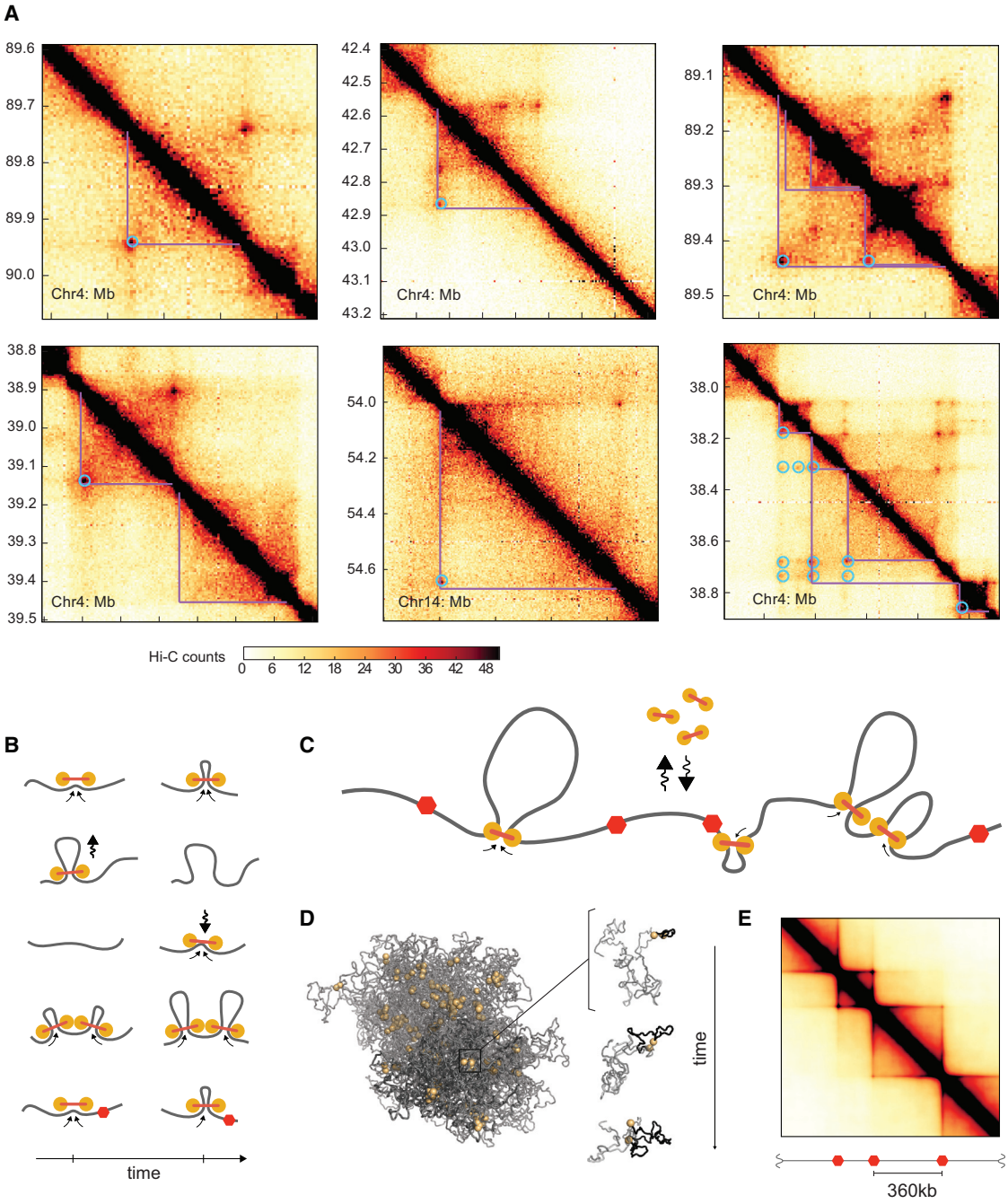

Figure 1. Loop Extrusion as a Mechanism for TAD Formation

(A) Hi-C contact maps at 5-kb resolution for six chromosomal regions (GM12878 in situ MboI) (Rao et al., 2014), highlighting TADs (purple lines) and peak loci (blue circles).

(B) Model of LEF dynamics (Figure S1A): LEFs shown as linked pairs of yellow circles, chromatin fiber shown in gray. From top to bottom: extrusion, dissociation, association, stalling upon encountering a neighboring LEF, stalling at a BE (red hexagon).

(C) Schematic of LEF dynamics (Movies S1 and S2).

(D) Conformation of a polymer subject to LEF dynamics, with processivity 120kb, separation 120kb. Left: LEFs (yellow) and chromatin (gray), for one conformation, where darker gray highlights the combined extent of three regions of sizes (180 kb, 360 kb, and 720 kb) separated by BEs. Right: the progressive extrusion of a loop (black) within a 180-kb region.

(E) Simulated contact map for processivity 120 kb and separation 120 kb.

TADs. One proposed mechanism giving good agreement to the observed TAD organization relies on supercoiling (Benedetti et al., 2014). Still, the connection between supercoiling and higher order eukaryotic chromosome organization remains unclear, since the reported agreement between supercoiling domain boundaries and TAD boundaries is roughly one in ten (Naughton et al., 2013).

Here, we propose a mechanism whereby TADs are formed by loop extrusion (Alipour and Marko, 2012; Nasmyth, 2001). In this process, *cis*-acting loop-extruding factors (LEFs; likely, cohesins) form progressively larger loops but are stalled by boundary elements (BEs), such as bound CTCF at TAD boundaries (Figures 1B and 1C). We tested this mechanism using polymer simulations of the chromatin fiber subject to the activity of LEFs. We found that it can produce TADs that quantitatively and qualitatively agree with Hi-C data. Importantly, our work provides a mechanism for preferentially forming contacts within TADs, such a mechanism is implicitly assumed in structural models of TADs formed by dynamic loops (Giorgetti et al., 2014; Hofmann and Heermann, 2015). Loop extrusion (Alipour and Marko, 2012), first introduced as processive loop enlargement by condensin (Nasmyth, 2001), has been implicated in mitotic chromosome compaction (Goloborodko et al., 2015; Naumova et al., 2013) and chromosome segregation in bacteria (Gruber, 2014; Wang et al., 2015). Importantly, however, these previous proposals did not consider any role of loop extrusion for TAD formation in interphase and did not directly test the impact of loop extrusion on 3D spatial organization or contact maps.

RESULTS

Mechanism of Loop Extrusion with BEs

To demonstrate how loop extrusion can lead to the formation of TADs, we first defined the dynamics of LEFs limited by BEs (Figures 1B and 1C; Figure S1A). Upon binding to the chromatin fiber, each LEF holds together two directly adjacent regions; then, it extrudes a loop by translocating along the chromatin fiber in both directions, holding together progressively more distant regions of a chromosome. Translocation stops when the LEF encounters an obstacle, either another LEF or a BE. If halted only on one side, LEFs continue to extrude on the other side. Throughout this process, LEFs can stochastically dissociate, releasing the extruded loop; for generality, we assume that this occurs uniformly across the genome. BEs underlie the formation of TADs by stalling LEF translocation, thus ensuring that extruded loops do not cross TAD boundaries. BEs in vivo might be formed by specifically bound architectural proteins, including CTCF, or any other impediment to LEF translocation. We note that BEs in vivo may be partially permeable because they either stochastically stall LEFs or are present in a fraction of cells.

Minimal 3D Model of Interphase Loop Extrusion

To efficiently explore how loop-extrusion dynamics spatially organize an interphase chromosome, we first studied a minimal model. In particular, we modeled a 10-Mb region of the chromatin fiber as a polymer subject to the activity of associating and dissociating LEFs limited by impermeable BEs (Figure 1C). As described previously (Naumova et al., 2013), we modeled the chromatin fiber as a polymer of 10-nm monomers (roughly three nucleosomes, or 600 bp) with excluded volume interactions and without topological constraints, subject to Langevin dynamics in OpenMM (Eastman et al., 2013). LEFs impose a system of bonds on the polymer: a bound LEF forms a bond between monomers at the two ends of an extruded loop, and the bond is re-assigned to increasingly separated pairs of monomers as a LEF translocates along the chromosome; when a LEF unbinds, this bond is removed. BEs, which halt LEF translocation, were placed at fixed positions, with sequential separations of 180 kb, 360 kb, and 720 kb through the 10-Mb region.

The dynamics of loop extrusion are determined by two independent parameters (Figure 2B; Figures S1B and S2): the average linear *separation* between bound LEFs, and the LEF *processivity*, i.e., the average size of a loop extruded by an unobstructed LEF over its lifetime (Goloborodko et al., 2015). Our model is additionally characterized by parameters governing the diffusivity of chromatin, polymer stiffness, density, and the Hi-C capture radius. For each set of parameter values, we ran polymer simulations long enough to allow $\geq$10 association/dissociation events per LEF (Movies S1 and S2). From simulations, we obtain an ensemble of chromosome conformations (Figure 1D) and compute the average contact frequency maps ("simulated Hi-C"; Figure 1E) that can be compared with experimental Hi-C data.

For many values of LEF processivity and separation, we observed the formation of TADs on a simulated Hi-C map (Figures 2C–2F). For some parameter values, we observed the formation of homogenous TADs; other simulated parameter sets led to the formation of peaks at corners of TADs, or enrichment of contacts at the boundary of TADs, seen as lines along the edge of a TAD. These simulations illustrate how the combined action of LEFs and BEs leads to enrichment of interactions within TADs and effective insulation between neighboring TADs.

TADs Are Formed by Dynamic Loops

Next, we tested the ability of our model to reproduce the Hi-C contact frequency as a function of genomic distance *s* (*P(s)*), used previously for quantifying polymer models (Barbieri et al., 2012; Benedetti et al., 2014; Le et al., 2013; Naumova et al., 2013; Rosa et al., 2010). We aimed to reproduce the *P(s)* within TADs of sizes 180 kb, 360 kb, and 720 kb, as well as *P(s)* between TADs. We determined the goodness of fit for each parameter set as the geometric standard deviation of the ratios of the four experimental and four simulated *P(s)* curves (see Experimental Procedures). Note that *P(s)* between TADs is ~2-fold smaller and scales differently with distance (Figure 2A; Figure S2C). For each pair of values of LEF processivity and LEF separation, we quantified the best achieved goodness of fit and the number of times a pair appears among the top 100 out of 6,912 total parameter sets (Figure 2B).

We found that the best agreement with Hi-C data is achieved for LEF processivity of ~120–240 kb and LEF separation of ~120 kb (Figure 2B), where the resulting TADs consist of dynamically forming, growing, and dissociating loops (Figure 3A; Figures S1E–S1G). In this regime, LEFs extrude ~75-kb loops relatively independently, as there are substantial gaps between LEFs (52%–69% average coverage of TADs by loops).

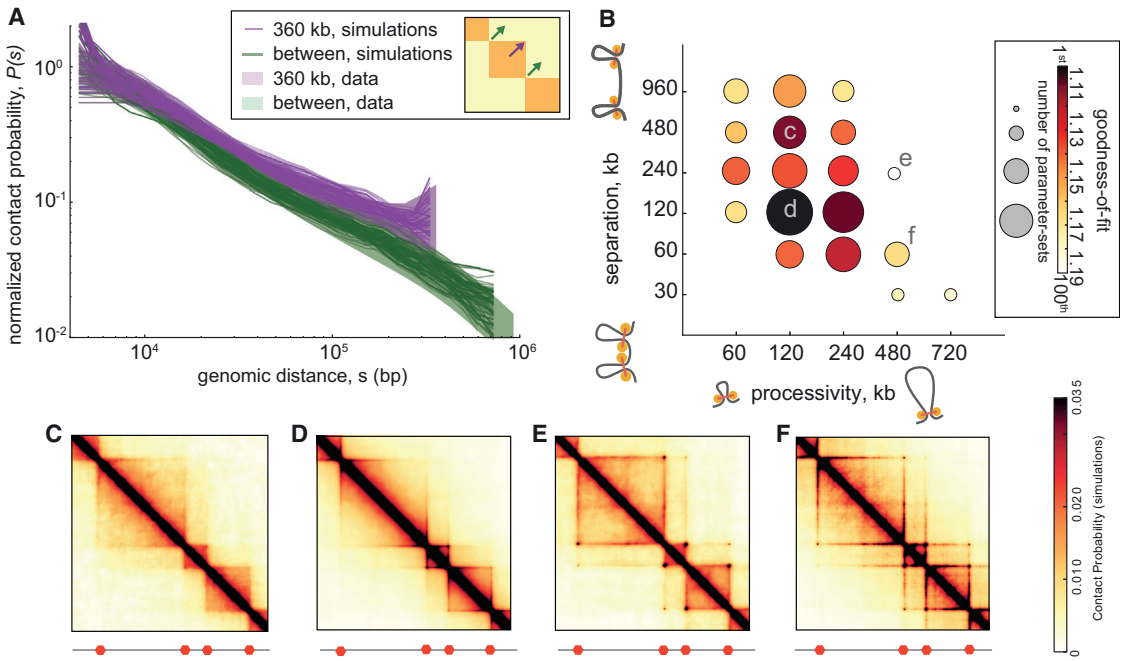

Figure 2. Quantitative Analysis of Loop Extrusion

(A) Experimental *P(s)* (shaded areas) versus simulated *P(s)* for the 100 best fitting parameter sets (lines, one per parameter set) within TADs (purple) and between TADs (green). Experimental *P(s)* calculated from 2-kb contact maps and normalized to one at 4 kb; shaded area shows 10th and 90th percentiles at each genomic distance. Simulated *P(s)* shown with vertical offsets from fitting (Experimental Procedures).

(B) Goodness of fit versus LEF processivity and separation for the 100 best fitting parameter sets (from 6,912 total parameter sets; Data S1). Circled areas represent the number of parameter sets among the top 100, while color quantifies the best fit at each processivity-separation pair; a value of 1 indicates a perfect fit.

(C–F) Simulated contact maps for the indicated processivity-separation pairs.

Notably, TADs are barely visible in simulated single-cell contact maps (Figure 3B). Moreover, only a small fraction of contacts on the map are directly mediated by LEFs. Consistently, polymer conformations display high spatial overlap between adjacent TADs, rather than appearing as segregated globules (Figure 3C; Figure S3A). Indeed, in both simulated and experimental Hi-C maps, there is only a ~2-fold depletion of contacts between neighboring TADs (Figure 2A; Figure S2C). Together, this demonstrates how TADs emerge as a population-average feature.

Loop Extrusion Recapitulates Results of Experimental TAD Boundary Deletions

Importantly, the mechanism of loop extrusion naturally recapitulates the results of TAD boundary deletion experiments (Nora et al., 2012). Upon the experimental deletion of a TAD boundary, the TAD spreads to the next boundary; this indicates that preferential interactions between loci in a TAD are not hard-wired and that BEs play crucial roles. This behavior has been confirmed with targeted disruption of CTCF-binding motifs at TAD boundaries (Guo et al., 2015; Narendra et al., 2015; Sanborn et al., 2015; de Wit et al., 2015). Consistently, in our model, deletion of a BE leads to spreading of a TAD until the next BE (Figure S1C).

TAD Corner-Peaks Are Not Permanent Loops

Many TADs appear to have peaks of interactions at their corners in Hi-C data (~50%; Rao et al., 2014). Interestingly, we found that TADs with and without peaks have similar *P(s)*, suggesting a similar underlying organizational mechanism, independent of the corner peak (Figure S2C). In agreement, our model shows that the mechanism of loop extrusion can produce both types of TADs, as increasing LEF processivity naturally strengthens peaks at TAD corners (Figures 2E and 2F; Figure S2A). Interestingly, our simulations show that TADs with visibly strong peaks do not require permanent contact between BEs, in agreement with our analyses of Hi-C data (Figures S4F and S4G).

Our simulations, together with previous polymer studies of chromatin loops (Benedetti et al., 2014; Doyle et al., 2014; Hofmann and Heermann, 2015), demonstrate that single stable loops are incapable of producing TADs. As follows, we refrain from directly identifying TAD corner peaks with loops. Indeed, we found that stable loops between BEs provide some of the worst fits to Hi-C data, with exceedingly strong corner peaks and a lack of visible TADs (Figure 4; Figure S4D). This stands in contrast with popular depictions of TADs as loops (Rao et al., 2014). Instead, our model predicts that TADs with and without corner peaks result from the collective activity of LEFs in the region between BEs.

TADs Require Long-Range Insulation

Importantly, insulation between neighboring TADs in our model does not arise from direct physical blocking of interactions by BEs. Instead, our model relies on the ability of BEs to regulate the translocation of LEFs. LEFs allow for insulation to be

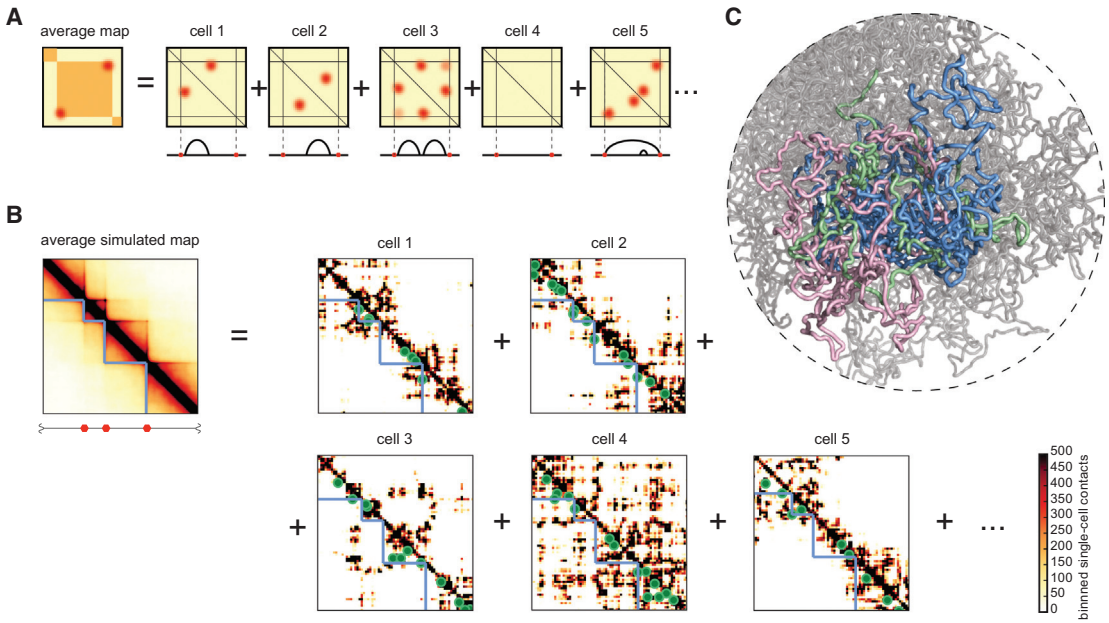

Figure 3. TADs Formed by LEFs Consist of Dynamically Forming, Growing, and Dissociating Loops

(A) Illustration of how TADs formed by loop extrusion result from averaging the dynamic positions of loop bases over many cells, including configurations with nested (cell 5) and consecutive (cell 3) loops (Figure S1).

(B) Left: the simulated contact map, as in Figure 1E, is an average of many single-cell maps. Right: simulated single-cell contact maps (18-kb resolution; green circles show LEF positions).

(C) Conformation of a polymer subject to LEF dynamics with processivity at 120 kb and separation at 120 kb. Three neighboring TADs of 180 kb, 360 kb, and 720 kb colored in green, pink, and blue, respectively. Contacts from an ensemble of such conformations are averaged together to form a contact map.

mediated over spatial and genomic distances much larger than the physical size of the BE. To rule out the possibility that a bulky BE is sufficient to insulate neighboring TADs, we performed simulations of this scenario. Indeed, in simulations where a BE is simply a bulky object, we see no long-range insulation and fail to obtain TADs (Figure 5; Figure S5). Similarly, in simulations where the chromatin fiber is locally very stiff at a BE, we again only see local insulation and fail to obtain TADs. Together, these simulations highlight the role of LEFs for imposing insulation at the scale of whole TADs.

Another important characteristic of our model is that loops extruded by LEFs act in *cis*, along the chromatin fiber, and do not impose interactions between genomically distal loci or loci on different chromosomes. Indeed, when we analyzed the interaction patterns of peak loci in Hi-C data, we found that there was no enrichment of contacts between pairs of peak loci at larger separations on the same chromosome or between different chromosomes (Figures S5G and S5H). This pattern is consistent with our model but is inconsistent with models that rely on direct interactions between BEs when such loci come into spatial proximity.

To rule out the mechanism whereby TADs are formed by direct BE-to-BE associations, we performed simulations where any two BEs would interact when they came into close spatial proximity (Figures S5I–S5L). Biologically, this represents a scenario where proteins interact to bridge cognate genomic elements (Barbieri et al., 2012; Bohn and Heermann, 2010; Brackley et al., 2015; Scolari and Cosentino Lagomarsino, 2015), for example, via interactions mediated by dimerization of bound CTCF. Our simulations confirmed that a direct BE-to-BE mechanism has no way of distinguishing between distant or proximal chromosomal regions; instead, all pairs of BEs display peaks of contact probability. Moreover, direct BE-to-BE interactions alone imposed negligible insulation between neighboring TADs, even in the case of strongly interacting BEs. Together, these results demonstrate the utility of LEFs stalled by BEs for restricting potentially interacting pairs of loci to those that are within TADs.

Molecular Roles for Cohesin and CTCF as LEFs and BEs

Next, we investigated possible molecular candidates for LEFs and BEs for TAD formation in interphase. We found that our proposed roles of cohesin as a LEF and CTCF as a BE both reconcile existing experimental results and predict outcomes of future experiments.

Multiple lines of evidence point to cohesin as a possible LEF in interphase. Like condensin, cohesin is a Structural Maintenance of Chromosomes (SMC) complex. These have been hypothesized to extrude chromatin loops (Alipour and Marko, 2012; Nasmyth, 2001), have similar molecular architectures to known motor proteins (Guacci et al., 1993; Nasmyth, 2001; Peterson, 1994), and have very recently been shown to slide along DNA (Stigler et al., 2016). Cohesins have been implicated in interphase TAD organization (Mizuguchi et al., 2014; Sofueva et al., 2013; Zuin et al., 2014) and chromatin looping (Kagey et al., 2010) beyond their role in sister chromatid cohesion. Indeed,

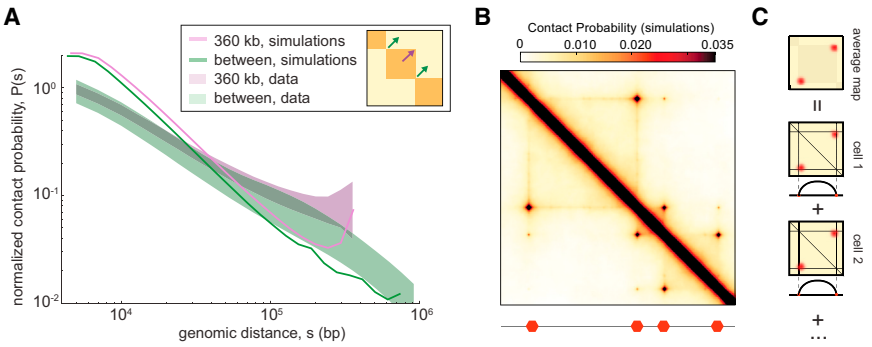

Figure 4. Simple Strong Loops Are Not TADs

(A) Experimental *P(s)* (shaded areas) versus simulated *P(s)* (solid lines) for a parameter set with a strong loop between neighboring BEs, calculated as in Figure 2A. Here, the fit is relatively poor (1.4137, rank 2,208 out of 6,912), and loops are not completely permanent, with BEs in contact 27% of the time for the 180-kb TAD and 14% of the time for the 720-kb TAD.

(B) Simulated contact map for a simple strong loop with processivity at 960 kb and separation at 960 kb.

(C) Illustration of how a single loop present in many cells leads to strong corner-peaks between neighboring BEs.

cohesins dynamically bind chromatin even before DNA replication (Gerlich et al., 2006). Finally, cohesin is enriched at interphase TAD boundaries (Dixon et al., 2012) and corner peaks (Rao et al., 2014), and its depletion makes TADs less prominent (Sofueva et al., 2013; Zuin et al., 2014).

CTCF is a similarly relevant molecular candidate for forming BEs. First, CTCF is enriched at TAD boundaries (Dixon et al., 2012), its depletion makes TADs less prominent (Zuin et al., 2014), and it has a relatively long residence time on chromatin (Nakahashi et al., 2013). Second, bound CTCF interacts with cohesin (Parelho et al., 2008) in an orientation-dependent manner (Xiao et al., 2011), similar to the interactions of shugoshin (Hara et al., 2014) and sororin (Nishiyama et al., 2010) with cohesin. Third, inward-oriented CTCF sites are enriched at TAD boundaries (Vietri Rudan et al., 2015) and TAD corner-peaks (Rao et al., 2014). We note that any impediment to LEF translocation may serve as a BE. As follows, BEs in vivo may be formed by sites with high occupancy of proteins other than CTCF (Van Bortle et al., 2014) that block LEF translocation physically rather than through a specific interaction. For example, active promoters bound by transcription-associated machinery are prominent candidates, as they are particularly bulky and are enriched at TAD boundaries (Dixon et al., 2012; Ulianov et al., 2016).

Loop Extrusion Predicts the Effects of Cohesin and CTCF Perturbations

The proposed roles of cohesin as a LEF and CTCF as a BE make predictions for patterns of cohesin and CTCF binding, genomic engineering experiments at particular loci, and global perturbations of cohesin and CTCF levels on chromosomal organization. First, analogous to LEF accumulation at BEs in our simulations (Figure 6B), we predict that cohesin accumulates at CTCF-binding sites but only when CTCF is bound at these sites (Parelho et al., 2008). Consistently, we find that cohesin chromatin immunoprecipitation sequencing (ChIP-seq) peaks are more enriched around strongly bound CTCF peaks (Figures 6C and 6D). This suggests that CTCF binding strength can translate into BE permeability.

Second, with these molecular roles, our simulations make predictions about changes in contact maps and spatial distances that would result from experimental perturbations to cohesin and CTCF (Figure S2). In particular, we predict that depletion of CTCF will result in increased permeability of BEs, thus reducing insulation between neighboring TADs, yet would have little effect on spatial distances of loci within TADs and only moderately reduce spatial distances of loci between TADs. In contrast, depletion of cohesin, modeled as an increased LEF separation, would also make TADs weaker but would be accompanied by more drastic increases of distances for loci both within and between TADs. Currently available Hi-C data support such differential, non-redundant, effects of CTCF and cohesin depletion on Hi-C maps (Zuin et al., 2014). Consistently, available imaging data support decompaction following cohesin depletion (Nolen et al., 2013; Sofueva et al., 2013; Zuin et al., 2014) and lack of decompaction following CTCF depletion (Nolen et al., 2013). Finally, our model predicts that greatly increased cohesin-binding time, modeled as greatly increased LEF processivity, would condense interphase chromosomes into a prophase-like "vermicelli" state (Figure S3), as seen upon depletion of the cohesin unloader Wapl (Tedeschi et al., 2013).

Complex TAD Architectures from Directional CTCF Boundaries

If bound CTCFs act as directional BEs, stopping LEF translocation from one side only, then the mechanism of loop extrusion can also explain the observed enrichment in convergent CTCF sites at TAD boundaries and loop bases, even at very large genomic separations (Figure 6A; Figure S6). Loop extrusion with directional BEs also provides a rationale for the results of manipulating CTCF site orientation, where flipping solely the orientation of a CTCF site can cause two neighboring TADs to merge (Guo et al., 2015; Narendra et al., 2015; Sanborn et al., 2015; de Wit et al., 2015). Interestingly, CTCF-binding sites at TAD boundaries are oriented so that the C terminus of bound CTCF (Nakahashi et al., 2013), known to interact with cohesin (Xiao et al., 2011), faces the interior of TADs. Indeed, we found that cohesin ChIP-seq peaks are enriched in this exact orientation-dependent manner around strongly bound CTCF peaks (Figures 6C–6F). Interestingly, YY1 and Znf143 were also enriched around strongly bound CTCF peaks, but only the former displayed an orientation dependence similar to cohesin. Together, these observations support a mechanism where CTCF acts as a BE that impedes loop extrusion by cohesins in an orientation-dependent manner.

To further test whether CTCF as a directional BE can recapitulate the variety of TAD domain architectures in vivo, we extended the minimal model introduced earlier to investigate a complex system of directional BEs with locus-specific

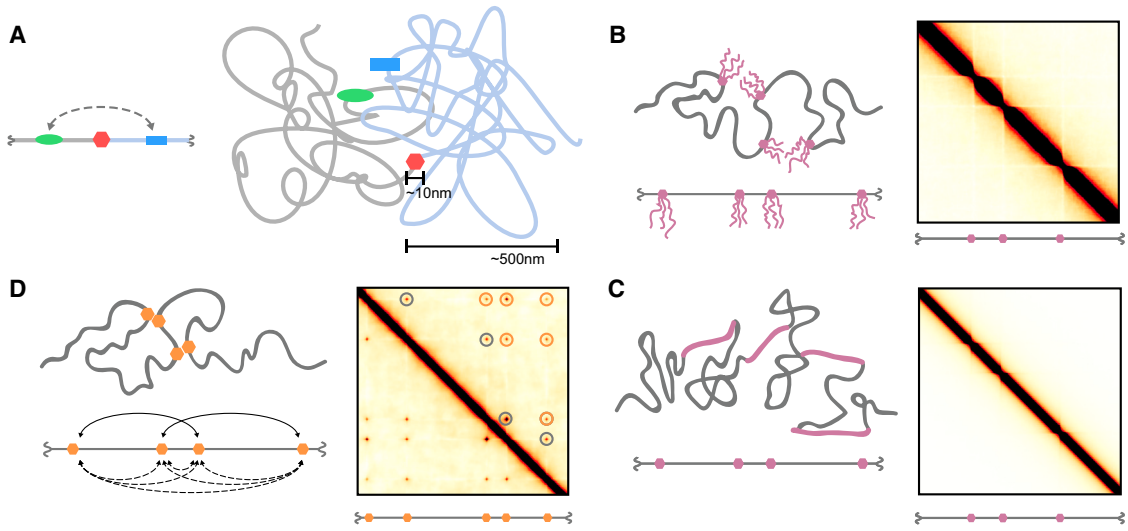

Figure 5. TADs Require Long-Range Insulation

(A) Illustration of a genomic region with an insulating element (red hexagon), a promoter (blue rectangle), and an enhancer (green oval) in 1D and 3D (Supplemental Notes).

(B) Illustration and contact map for a model of BEs as large bulky objects (e.g., bound by proteins or RNA). Each BE is bound by three polymer chains of length 10.

(C) As above, for a model of BEs as a stiff region of chromatin (ten monomers of stiffness 6).

(D) As above, for a model with direct BE-to-BE attraction (attraction strength 3). Solid arcs display interactions in this particular conformation, and dashed arcs show all possible interaction partners. Black circles indicate peaks between neighboring BEs, and orange circles indicate peaks between non-neighboring BEs.

permeability (Figure 7). For these simulations, we converted ChIP-seq data for CTCF over a 15-Mb region of human chromosome 14 (chr14) into BE permeability and directionality. First, since many CTCF peaks are not uniquely associated with a motif, we assigned directionality for ambiguous CTCF peaks using the nearest cohesin peak. Second, we transformed CTCF ChIP-seq peak heights into BE permeability using a logistic function such that more weakly bound CTCF sites formed more permeable BEs. We found that when the parameters of the best-fitting minimal model were used, this system produced contact maps with good agreement with Hi-C maps at short distances (<400 kb) but poor agreement at further distances (Figure S7). We found that better agreement at far distances can be obtained if we increased LEF processivity to 360 kb (corresponding to an increase in average loop size from ~75 kb to ~135 kb). Still, even with increased LEF processivity, agreement along the chromosome was non-uniform (Figure S7).

Upon inspecting these simulated maps (Figure 7; Figure S7), we noticed that strong CTCF sites tended to produce stronger boundaries, both in simulations and in the Hi-C data, while weak CTCF sites (e.g., 66.5 Mb) had minimal effects on both maps. Consistently, CTCF sites that are not at annotated TAD boundaries have lower CTCF occupancy (Figure S6D). In both maps, CTCF-depleted regions formed large homogenous domains (e.g., chr14:62.6–63.6 Mb). Moreover, we found that our simulations recapitulated several other features of TAD organization, including: nested TADs (e.g., 62 Mb), strong interactions between the BE and the body of the domain ("lines" at the edge, or perimeter, of the TAD, e.g., 65.9 Mb), and complex networks of interactions between several BEs ("grids" of peaks, e.g., 66 Mb). These results illustrate how not only TADs but also finer structures similar to those found in experimental Hi-C maps naturally emerged in our simulations without being directly encoded; this further supports loop extrusion as a mechanism of chromosomal organization in interphase.

DISCUSSION

In summary, our model of loop extrusion not only forms TADs in agreement with Hi-C but also agrees with a number of specific features observed experimentally. First, loop extrusion naturally produces enrichment of contacts within a domain and can create corner peaks between TAD boundaries. Second, loop extrusion naturally explains finer structures, including nested TADs, lines at TAD edges, and grids of peaks. Third, it explains why peaks of interactions are absent between distal BEs and BEs on different chromosomes. Fourth, it explains the merging of TADs seen in boundary deletion experiments. Fifth, it provides a rationale for inward-oriented CTCF motifs at TAD boundaries. Sixth, it explains a directional bias in the accumulation of cohesin peaks around bound CTCF motifs. Seventh, it is consistent with current Hi-C and microscopy results for CTCF and cohesin depletion. Finally, it allows for interaction peaks between BEs that are not simple stable loops, as necessary for consistency with available Hi-C and microscopy data (Imakaev et al., 2015). Given the ability of loop extrusion to recapitulate complex locus-specific folding patterns, we propose that TADs may be better understood as one of many emergent phenomena from loop extrusion, rather than a discrete and distinct set of genomic entities.

Loop extrusion as a model of TAD formation in interphase has recently received a significant amount of attention. In Nichols and Corces (2015), the authors proposed, but did not quantitatively

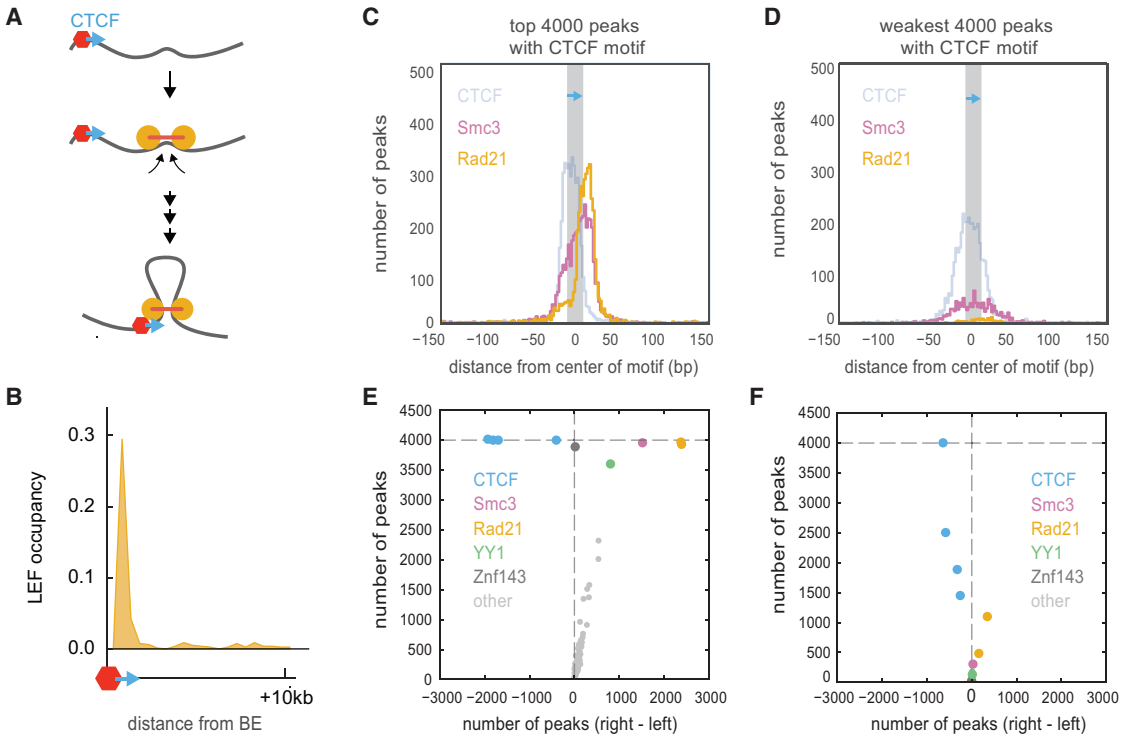

Figure 6. CTCF as a Directional BE

(A) Inward-oriented CTCF sites at TAD boundaries are consistent with loop extrusion and a directional boundary function of CTCF (Figure S6).

(B) Accumulation of LEFs at BEs for simulations with processivity at 120 kb and separation at 120 kb.

(C) Distributions of CTCF, Smc3, and Rad21 ChIP-seq peak summits in the vicinity of the 4,000 strongest motif-associated CTCF binding peaks (orientation indicated by blue arrow).

(D) Same as in (C), but for the weakest 4000 motif-associated CTCF-binding sites.

(E) Asymmetry and enrichment of factor ChIP-seq peak summits around the strongest 4,000 motif-associated CTCF sites. Each dot represents an ENCODE GM12878 ChIP-seq track. The y axis shows the number of peaks within ±200 bp of a CTCF motif. The x axis shows the difference between the number of peak summits on the right and on the left of the motif, i.e., asymmetry of the factor relative to a CTCF motif.

(F) Same, but for the weakest 4,000 motif-associated CTCF ChIP peaks.

test, that bound CTCF can load cohesin in an orientation-specific manner, holding one side of the cohesin complex while the other translocates to form an extruded loop. We note that, if the majority of cohesin is loaded in this fashion, the results of cohesin depletion would be similar to those of CTCF depletion, in contrast with current experimental results reporting non-redundant effects (Zuin et al., 2014); in the context of loop extrusion, details of LEF loading and BE function are important subjects for future study. In Sanborn et al. (2015), published while our manuscript was available as a preprint (http://biorxiv.org/content/early/2015/08/14/024620), the authors considered a tension globule model as well as a loop extrusion model similar to the one presented here. Surprisingly, for both the tension globule and the loop extrusion models, they found good agreement with experimental *P(s)* that is robust to changes in simulation parameters. In contrast, for loop extrusion we found that *P(s)* depends strongly on the parameters of LEF dynamics. This may be because we considered a wider range of LEF processivities and separations, spanning from a free-polymer regime to a permanent loop regime, to a compacted "vermicelli" regime. Also, in contrast with Sanborn et al. (2015), where 13 out of 13 genomic engineering experiments were successfully predicted, we found a non-uniform agreement as a function of genomic position between the results of our simulations and Hi-C maps. We believe that our observation of non-uniform agreement along the chromosome can reflect: additional undetermined factors underlying BEs, locus-specific details of LEF dynamics (including sites of loading and unloading), the role of higher-order active and inactive compartments (Brackley et al., 2015; Jost et al., 2014) and lamina associations (Kind et al., 2015), or locus-specific experimental details of Hi-C and ChIP-seq (Imakaev et al., 2012; Yaffe and Tanay, 2011).

Consideration of a wide range of LEF processivities and separations allowed us to make predictions regarding the effects of CTCF and cohesin perturbations. Indeed, our simulations predict distinct consequences of CTCF and cohesin depletion on Hi-C maps and spatial distances, consistent with available imaging and Hi-C data (Nolen et al., 2013; Sofueva et al., 2013; Zuin et al., 2014). Still, further validation of our predictions requires new methods for architectural protein removal, as available techniques have yet to fully disrupt TAD formation. Additionally, we note that other proteins complexes may play important roles in chromosome organization, potentially via mechanisms distinct from loop extrusion; for example, bound polycomb may be able to self-associate, thus compacting polycomb-bound

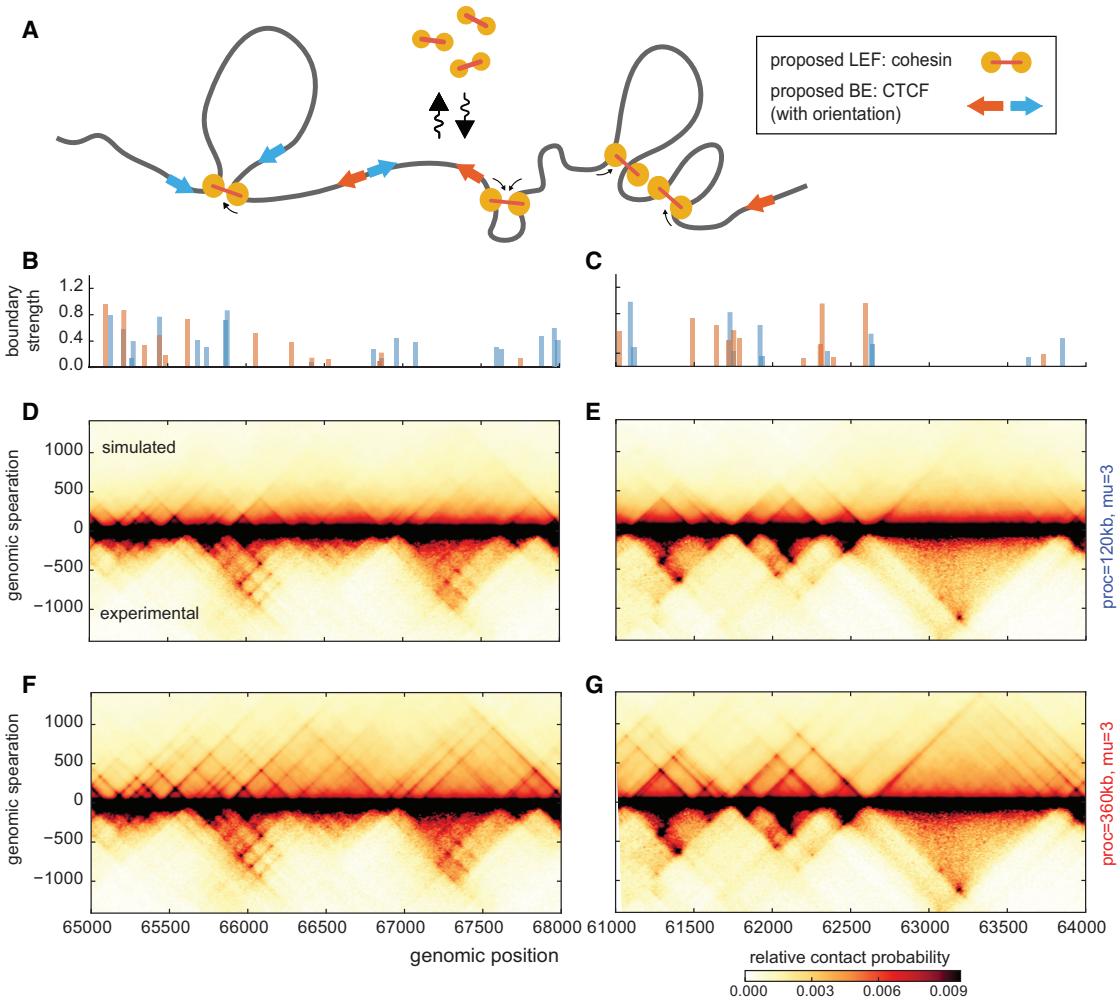

Figure 7. Complex TAD Architectures from Loop Extrusion

(A) Schematic of LEF dynamics with directional BEs.

(B and C) Directional BE strength profile (the sum of BEs occupancies within a 12-kb bin) for regions simulated in (D–G).

(D–G) Simulated contact maps for regions of human chr14, GM12878 cell type, for models with orientation-specific BEs of varying permeability. Maps are compared with experimental maps for the same regions at the same 12-kb resolution (Figure S7). LEF processivity is 120 kb (D and E) and 360 kb (F and G).

regions (Boettiger et al., 2016) and possibly contributing to the formation of TAD-like domains (Williamson et al., 2014).

The mechanism of loop extrusion in interphase has additional, potentially far-ranging, consequences for processes in the nucleus. First, enhancer-promoter pairings can be dictated by the relative placement of BEs, including CTCF (Hou et al., 2008). Second, loop extrusion may have an even stronger effect if LEFs stall at promoters, effectively turning the enhancer-promoter search process into a 1D search process and allowing for orientation-specific interactions. Third, loop extrusion may facilitate high-fidelity VDJ and class-switch recombination, as well as other processes dependent on long-range intra-chromosomal looping with specific orientations, particularly given the observed interplay between CTCF and cohesin (Alt et al., 2013; Degner et al., 2011; Dong et al., 2015; Lin et al., 2015).

Finally, the mechanism of TAD formation via loop extrusion studied here is similar to the proposed mechanism of mitotic chromosome condensation (Alipour and Marko, 2012; Goloborodko et al., 2015, 2016; Nasmyth, 2001; Naumova et al., 2013) but with the addition of BEs and many fewer, less processive, LEFs. Accordingly, increasing the number and processivity of LEFs and removing BEs could underlie the transition from interphase to mitotic chromosome organization. Conversely, upon exit from mitosis, interphase 3D chromosome organization can be re-established by restoring previous BE positions, which could potentially be epigenetically inherited bookmarks (Kadauke and Blobel, 2013).

EXPERIMENTAL PROCEDURES

LEF Dynamics with BEs

LEF translocation along a chromatin fiber was simulated on a 1D lattice, where each position was characterized by the following parameters: association (birth) probability, dissociation (death) probability, and BE occupancy (stalling probability). For the minimal model, we considered a system with uniform birth

probability, constant death probability, a fixed number of LEFs, and a discrete number of completely impermeable BEs. As described previously (Goloborodko et al., 2015), we modeled LEFs as having two "heads" connected by a linker.

3D Simulations

We represent chromatin fibers as a polymer of spherical monomers connected by harmonic bonds, with stiffness and a soft-core repulsive potential. Simulations were performed with Langevin dynamics in periodic boundary conditions using OpenMM (Eastman and Pande, 2010; Eastman et al., 2013). The two monomers held by the two heads of each LEF were connected by a harmonic bond. A 3D-to-1D dynamics parameter controlled the number of 3D-simulation time steps per 1D-simulation time steps.

Minimal 3D Polymer Model

We performed simulations of a polymer chain consisting of eight groups of three TADs of 300, 600, and 1,200 monomers each, arranged sequentially (300; 600; 1,200; 300; …). Impermeable BEs were placed between neighboring TADs. For each parameter set, we collected 2,000 conformations to calculate *P(s)* and 10,000 for contact maps.

Parameter Sweep

We considered the following values for the five simulation parameters:

LEF processivity: 100; 200; 400; 800; 1,200; 1,600
LEF separation: 50; 100; 200; 400; 800; 1,600
3D-to-1D dynamics: 300/4; 1,000/4; 5,000/4
Stiffness: 0; 2; 4; 6
Density: 0.05; 0.2.

For each of these 864 separate simulations, we generated 2,000 conformations (total: 1,728,000), and calculated contact maps for the eight values of the Hi-C capture radius (the distance at which contacts between two monomers are recorded; 2, 3, 4, 5, 6, 7, 8, and 10), for a total of 6,912 parameters sets.

Experimental P(s) *and Hi-C Maps*

To calculate experimental *P(s)* within and between TADs, we used publicly available data and annotations from Rao et al. (2014). Data were processed in house using *hiclib* (Imakaev et al., 2012) for the GM12878 inSitu protocol and MboI restriction enzyme, binned at 2 kb. Displayed Hi-C maps were at a 5-kb resolution, processed similarly.

Goodness of Fit

To compare experimental and simulated *P(s)*, we averaged over experimental TADs 0.9–1.1 of the size of a simulated TAD, (180 kb, 360 kb, and 720 kb). The goodness of fit was the geometric standard deviation of the ratio of simulated to experimental *P(s)*. Since the best fitting models had diverse parameter sets, we took the first 100 best fitting models (fit values, 1.103–1.195) and assessed how frequently each pair (processivity, separation) occurs in this list and what the best fit was for each pair.

ChIP-Seq Peaks around Oriented CTCF Motifs

Motifs were assigned to ENCODE narrow-peak calls in the GM12878 cell line by interval intersection, using bedtools (Quinlan and Hall, 2010). Genome-wide CTCF motif matches were also obtained from ENCODE (Kheradpour and Kellis, 2014), using the CTCF_known1 motif. For 4,000 most and least enriched CTCF peaks, we produced histograms of the summit positions of ENCODE-called ChIP peaks for other factors.

Converting CTCF ChIP-Seq to Orientation-Specific BE Permeability

To convert ChIP-seq peak strength to the occupancy of simulated BEs, we used a logistic transformation, $f(x) = 1/(1 + \exp(-x/20 - \mu))$, where x is a sum of peak fold-change-over-input values for peaks with a given orientation in a 600-bp bin. $\mu = 3$ was used as the default, and $\mu = 2$ or $\mu = 4$ was used for higher or lower CTCF occupancy. Peak orientation was determined by the motif orientation; when unavailable, we used relative orientation of CTCF and the closest Rad21 peak.

3D Polymer Model with Orientation-Specific BEs

We modeled a 15-Mb region of human chr14, 60,000,000 to 75,000,000, using the same parameters as the best fitting minimal model. We also considered simulations with different processivity and CTCF occupancy. The simulated contact map was rescaled to 12-kb resolution and compared to GM12878 in situ data from Rao et al. (2014), corrected at 10 kb, and rescaled to 12 kb.

Models of Direct BE-to-BE Interactions, Bulky and Stiff BEs

Models had the same BE positions as in the minimal model but did not include LEF dynamics. To simulate direct BE-to-BE interactions, we used an attractive soft-core potential. Contact maps were displayed for attractive strengths of 1.5, 3, and 5, and a contact radius of 10. For bulky BEs, several polymer chains were connected at each BE (either three chains of length 10 attached one per monomer to the monomers around the BE via harmonic bonds, or five chains of length 6). For stiff BEs, the 10 monomers around the BE had an increased stiffness of 6, while other monomers had a stiffness of 1, as defined earlier.

SUPPLEMENTAL INFORMATION

Supplemental Information includes Supplemental Experimental Procedures, Supplemental Notes, seven figures, two movies, and one database file and can be found with this article online at http://dx.doi.org/10.1016/j.celrep.2016.04.085.

AUTHOR CONTRIBUTIONS

G.F., M.I., and L.A.M. conceived of the project and wrote the paper. C.L. performed initial simulations. N.A. led ChIP-seq and motif analyses. A.G. led literature curation for CTCF and cohesin. M.I. led polymer simulations. G.F. led experimental data analyses.

ACKNOWLEDGMENTS

M.I. and G.F. would like to thank the MIT PRIMES: Program for Research in Mathematics, Engineering, and Science for High School Students for the opportunity to supervise excellent students. This project began as C.L.'s project for the MIT PRIMES, supervised by M.I. and G.F., and initial results were presented at the annual PRIMES conference in May 2013 (https://math.mit.edu/research/highschool/primes/materials/2013/conf/12-2-Lu.pdf). Work including detailed comparison to experimental Hi-C data was presented at conferences in Heidelberg (May 2015) and at the Weizmann Institute (June 2015), and was available as a preprint at bioRxiv, August 2015 (http://biorxiv.org/content/early/2015/08/14/024620). The authors thank Job Dekker for many stimulating discussions. The authors also thank Edith Heard, Suzana Hadjur, Katerina Kraft, Elphege Nora, Francois Spitz, and other attendees of the Genome Regulation in 3D Conference at the Weizmann Institute for helpful discussions and feedback. We are thankful to Maxime Dahan for many productive discussions and Labex and Institut Curie for hosting L.M., G.F., and A.G. during this work. Authors are supported by grants R01 GM114190, U54 DK107980, and R01 G003143 from the National Institute of Health and 1504942 from the National Science Foundation.

Received: October 12, 2015
Revised: December 1, 2015
Accepted: April 20, 2016
Published: May 19, 2016

REFERENCES

Alipour, E., and Marko, J.F. (2012). Self-organization of domain structures by DNA-loop-extruding enzymes. Nucleic Acids Res. *40*, 11202–11212.

Alt, F.W., Zhang, Y., Meng, F.-L., Guo, C., and Schwer, B. (2013). Mechanisms of programmed DNA lesions and genomic instability in the immune system. Cell *152*, 417–429.

Andrey, G., Montavon, T., Mascrez, B., Gonzalez, F., Noordermeer, D., Leleu, M., Trono, D., Spitz, F., and Duboule, D. (2013). A switch between topological

domains underlies HoxD genes collinearity in mouse limbs. Science *340*, 1234167.

Barbieri, M., Chotalia, M., Fraser, J., Lavitas, L.-M., Dostie, J., Pombo, A., and Nicodemi, M. (2012). Complexity of chromatin folding is captured by the strings and binders switch model. Proc. Natl. Acad. Sci. USA *109*, 16173–16178.

Baù, D., Sanyal, A., Lajoie, B.R., Capriotti, E., Byron, M., Lawrence, J.B., Dekker, J., and Marti-Renom, M.A. (2011). The three-dimensional folding of the α-globin gene domain reveals formation of chromatin globules. Nat. Struct. Mol. Biol. *18*, 107–114.

Benedetti, F., Dorier, J., Burnier, Y., and Stasiak, A. (2014). Models that include supercoiling of topological domains reproduce several known features of interphase chromosomes. Nucleic Acids Res. *42*, 2848–2855.

Boettiger, A.N., Bintu, B., Moffitt, J.R., Wang, S., Beliveau, B.J., Fudenberg, G., Imakaev, M., Mirny, L.A., Wu, C., and Zhuang, X. (2016). Super-resolution imaging reveals distinct chromatin folding for different epigenetic states. Nature *529*, 418–422.

Bohn, M., and Heermann, D.W. (2010). Diffusion-driven looping provides a consistent framework for chromatin organization. PLoS ONE *5*, e12218.

Brackley, C.A., Johnson, J., Kelly, S., Cook, P.R., and Marenduzzo, D. (2015). Binding of bivalent transcription factors to active and inactive regions folds human chromosomes into loops, rosettes and domains. arXiv, arXiv: 1511.01848. http://arxiv.org/abs/1511.01848.

de Wit, E., Vos, E.S.M., Holwerda, S.J.B., Valdes-Quezada, C., Verstegen, M.J.A.M., Teunissen, H., Splinter, E., Wijchers, P.J., Krijger, P.H.L., and de Laat, W. (2015). CTCF binding polarity determines chromatin looping. Mol. Cell *60*, 676–684.

Degner, S.C., Verma-Gaur, J., Wong, T.P., Bossen, C., Iverson, G.M., Torkamani, A., Vettermann, C., Lin, Y.C., Ju, Z., Schulz, D., et al. (2011). CCCTC-binding factor (CTCF) and cohesin influence the genomic architecture of the Igh locus and antisense transcription in pro-B cells. Proc. Natl. Acad. Sci. USA *108*, 9566–9571.

Dixon, J.R., Selvaraj, S., Yue, F., Kim, A., Li, Y., Shen, Y., Hu, M., Liu, J.S., and Ren, B. (2012). Topological domains in mammalian genomes identified by analysis of chromatin interactions. Nature *485*, 376–380.

Dong, J., Panchakshari, R.A., Zhang, T., Zhang, Y., Hu, J., Volpi, S.A., Meyers, R.M., Ho, Y.-J., Du, Z., Robbiani, D.F., et al. (2015). Orientation-specific joining of AID-initiated DNA breaks promotes antibody class switching. Nature *525*, 134–139.

Doyle, B., Fudenberg, G., Imakaev, M., and Mirny, L.A. (2014). Chromatin loops as allosteric modulators of enhancer-promoter interactions. PLoS Comput. Biol. *10*, e1003867.

Eastman, P., and Pande, V. (2010). OpenMM: a hardware-independent framework for molecular simulations. Comput. Sci. Eng. *12*, 34–39.

Eastman, P., Friedrichs, M.S., Chodera, J.D., Radmer, R.J., Bruns, C.M., Ku, J.P., Beauchamp, K.A., Lane, T.J., Wang, L.P., Shukla, D., et al. (2013). OpenMM 4: a reusable, extensible, hardware independent library for high performance molecular simulation. J. Chem. Theory Comput. *9*, 461–469.

Gerlich, D., Koch, B., Dupeux, F., Peters, J.-M., and Ellenberg, J. (2006). Live-cell imaging reveals a stable cohesin-chromatin interaction after but not before DNA replication. Curr. Biol. *16*, 1571–1578.

Gibcus, J.H., and Dekker, J. (2013). The hierarchy of the 3D genome. Mol. Cell *49*, 773–782.

Giorgetti, L., Galupa, R., Nora, E.P., Piolot, T., Lam, F., Dekker, J., Tiana, G., and Heard, E. (2014). Predictive polymer modeling reveals coupled fluctuations in chromosome conformation and transcription. Cell *157*, 950–963.

Goloborodko, A., Marko, J.F., and Mirny, L. (2015). Chromosome compaction via active loop extrusion. Biophys J. *110*, 2162–2168.

Goloborodko, A.A., Imakaev, M., Marko, J., and Mirny, L. (2016). Compaction and segregation of sister chromatids via active loop extrusion. eLife. http://dx.doi.org/10.7554/eLife.14864.

Gorkin, D.U., Leung, D., and Ren, B. (2014). The 3D genome in transcriptional regulation and pluripotency. Cell Stem Cell *14*, 762–775.

Gruber, S. (2014). Multilayer chromosome organization through DNA bending, bridging and extrusion. Curr. Opin. Microbiol. *22*, 102–110.

Guacci, V., Yamamoto, A., Strunnikov, A., Kingsbury, J., Hogan, E., Meluh, P., and Koshland, D. (1993). Structure and function of chromosomes in mitosis of budding yeast. Cold Spring Harb. Symp. Quant. Biol. *58*, 677–685.

Guo, Y., Xu, Q., Canzio, D., Shou, J., Li, J., Gorkin, D.U., Jung, I., Wu, H., Zhai, Y., Tang, Y., et al. (2015). CRISPR inversion of CTCF sites alters genome topology and enhancer/promoter function. Cell *162*, 900–910.

Hara, K., Zheng, G., Qu, Q., Liu, H., Ouyang, Z., Chen, Z., Tomchick, D.R., and Yu, H. (2014). Structure of cohesin subcomplex pinpoints direct shugoshin-Wapl antagonism in centromeric cohesion. Nat. Struct. Mol. Biol. *21*, 864–870.

Hofmann, A., and Heermann, D.W. (2015). The role of loops on the order of eukaryotes and prokaryotes. FEBS Lett. *589* (*20 Pt A*), 2958–2965.

Hou, C., Zhao, H., Tanimoto, K., and Dean, A. (2008). CTCF-dependent enhancer-blocking by alternative chromatin loop formation. Proc. Natl. Acad. Sci. USA *105*, 20398–20403.

Imakaev, M., Fudenberg, G., McCord, R.P., Naumova, N., Goloborodko, A., Lajoie, B.R., Dekker, J., and Mirny, L.A. (2012). Iterative correction of Hi-C data reveals hallmarks of chromosome organization. Nat. Methods *9*, 999–1003.

Imakaev, M.V., Fudenberg, G., and Mirny, L.A. (2015). Modeling chromosomes: Beyond pretty pictures. FEBS Lett. *589* (*20 Pt A*), 3031–3036.

Jost, D., Carrivain, P., Cavalli, G., and Vaillant, C. (2014). Modeling epigenome folding: formation and dynamics of topologically associated chromatin domains. Nucleic Acids Res. *42*, 9553–9561.

Kadauke, S., and Blobel, G.A. (2013). Mitotic bookmarking by transcription factors. Epigenetics Chromatin *6*, 6.

Kagey, M.H., Newman, J.J., Bilodeau, S., Zhan, Y., Orlando, D.A., van Berkum, N.L., Ebmeier, C.C., Goossens, J., Rahl, P.B., Levine, S.S., et al. (2010). Mediator and cohesin connect gene expression and chromatin architecture. Nature *467*, 430–435.

Kheradpour, P., and Kellis, M. (2014). Systematic discovery and characterization of regulatory motifs in ENCODE TF binding experiments. Nucleic Acids Res. *42*, 2976–2987.

Kind, J., Pagie, L., de Vries, S.S., Nahidiazar, L., Dey, S.S., Bienko, M., Zhan, Y., Lajoie, B., de Graaf, C.A., Amendola, M., Fudenberg, G., Imakaev, M., Mirny, L.A., Jalink, K., Dekker, J., van Oudenaarden, A., and van Steensel, B. (2015). Genome-wide maps of nuclear lamina interactions in single human cells. Cell *163*, 134–147.

Lajoie, B.R., Dekker, J., and Kaplan, N. (2015). The hitchhiker's guide to Hi-C analysis: practical guidelines. Methods *72*, 65–75.

Le, T.B.K., Imakaev, M.V., Mirny, L.A., and Laub, M.T. (2013). High-resolution mapping of the spatial organization of a bacterial chromosome. Science *342*, 731–734.

Lieberman-Aiden, E., van Berkum, N.L., Williams, L., Imakaev, M., Ragoczy, T., Telling, A., Amit, I., Lajoie, B.R., Sabo, P.J., Dorschner, M.O., et al. (2009). Comprehensive mapping of long-range interactions reveals folding principles of the human genome. Science *326*, 289–293.

Lin, S.G., Guo, C., Su, A., Zhang, Y., and Alt, F.W. (2015). CTCF-binding elements 1 and 2 in the Igh intergenic control region cooperatively regulate V(D)J recombination. Proc. Natl. Acad. Sci. USA *112*, 1815–1820.

Lupiáñez, D.G., Kraft, K., Heinrich, V., Krawitz, P., Brancati, F., Klopocki, E., Horn, D., Kayserili, H., Opitz, J.M., Laxova, R., et al. (2015). Disruptions of topological chromatin domains cause pathogenic rewiring of gene-enhancer interactions. Cell *161*, 1012–1025.

Marko, J.F., and Siggia, E.D. (1997). Polymer models of meiotic and mitotic chromosomes. Mol. Biol. Cell *8*, 2217–2231.

Mizuguchi, T., Fudenberg, G., Mehta, S., Belton, J.-M., Taneja, N., Folco, H.D., FitzGerald, P., Dekker, J., Mirny, L., Barrowman, J., and Grewal, S.I. (2014).

Cohesin-dependent globules and heterochromatin shape 3D genome architecture in S. pombe. Nature *516*, 432–435.

Nakahashi, H., Kwon, K.R., Resch, W., Vian, L., Dose, M., Stavreva, D., Hakim, O., Pruett, N., Nelson, S., Yamane, A., et al. (2013). A genome-wide map of CTCF multivalency redefines the CTCF code. Cell Rep. *3*, 1678–1689.

Narendra, V., Rocha, P.P., An, D., Raviram, R., Skok, J.A., Mazzoni, E.O., and Reinberg, D. (2015). CTCF establishes discrete functional chromatin domains at the Hox clusters during differentiation. Science *347*, 1017–1021.

Nasmyth, K. (2001). Disseminating the genome: joining, resolving, and separating sister chromatids during mitosis and meiosis. Annu. Rev. Genet. *35*, 673–745.

Naughton, C., Avlonitis, N., Corless, S., Prendergast, J.G., Mati, I.K., Eijk, P.P., Cockroft, S.L., Bradley, M., Ylstra, B., and Gilbert, N. (2013). Transcription forms and remodels supercoiling domains unfolding large-scale chromatin structures. Nat. Struct. Mol. Biol. *20*, 387–395.

Naumova, N., Imakaev, M., Fudenberg, G., Zhan, Y., Lajoie, B.R., Mirny, L.A., and Dekker, J. (2013). Organization of the mitotic chromosome. Science *342*, 948–953.

Nichols, M.H., and Corces, V.G. (2015). A CTCF code for 3D genome architecture. Cell *162*, 703–705.

Nishiyama, T., Ladurner, R., Schmitz, J., Kreidl, E., Schleiffer, A., Bhaskara, V., Bando, M., Shirahige, K., Hyman, A.A., Mechtler, K., and Peters, J.M. (2010). Sororin mediates sister chromatid cohesion by antagonizing Wapl. Cell *143*, 737–749.

Nolen, L.D., Boyle, S., Ansari, M., Pritchard, E., and Bickmore, W.A. (2013). Regional chromatin decompaction in Cornelia de Lange syndrome associated with NIPBL disruption can be uncoupled from cohesin and CTCF. Hum. Mol. Genet. *22*, 4180–4193.

Nora, E.P., Lajoie, B.R., Schulz, E.G., Giorgetti, L., Okamoto, I., Servant, N., Piolot, T., van Berkum, N.L., Meisig, J., Sedat, J., et al. (2012). Spatial partitioning of the regulatory landscape of the X-inactivation centre. Nature *485*, 381–385.

Parelho, V., Hadjur, S., Spivakov, M., Leleu, M., Sauer, S., Gregson, H.C., Jarmuz, A., Canzonetta, C., Webster, Z., Nesterova, T., et al. (2008). Cohesins functionally associate with CTCF on mammalian chromosome arms. Cell *132*, 422–433.

Peterson, C.L. (1994). The SMC family: novel motor proteins for chromosome condensation? Cell *79*, 389–392.

Quinlan, A.R., and Hall, I.M. (2010). BEDTools: a flexible suite of utilities for comparing genomic features. Bioinformatics *26*, 841–842.

Rao, S.S.P., Huntley, M.H., Durand, N.C., Stamenova, E.K., Bochkov, I.D., Robinson, J.T., Sanborn, A.L., Machol, I., Omer, A.D., Lander, E.S., and Aiden, E.L. (2014). A 3D map of the human genome at kilobase resolution reveals principles of chromatin looping. Cell *159*, 1665–1680.

Rosa, A., and Everaers, R. (2008). Structure and dynamics of interphase chromosomes. PLoS Comput. Biol. *4*, e1000153.

Rosa, A., Becker, N.B., and Everaers, R. (2010). Looping probabilities in model interphase chromosomes. Biophys. J. *98*, 2410–2419.

Sanborn, A.L., Rao, S.S.P., Huang, S.-C., Durand, N.C., Huntley, M.H., Jewett, A.I., Bochkov, I.D., Chinnappan, D., Cutkosky, A., Li, J., et al. (2015). Chromatin extrusion explains key features of loop and domain formation in wild-type and engineered genomes. Proc. Natl. Acad. Sci. USA *112*, E6456–E6465.

Scolari, V.F., and Cosentino Lagomarsino, M. (2015). Combined collapse by bridging and self-adhesion in a prototypical polymer model inspired by the bacterial nucleoid. Soft Matter *11*, 1677–1687.

Sexton, T., Yaffe, E., Kenigsberg, E., Bantignies, F., Leblanc, B., Hoichman, M., Parrinello, H., Tanay, A., and Cavalli, G. (2012). Three-dimensional folding and functional organization principles of the Drosophila genome. Cell *148*, 458–472.

Stigler, J., Çamdere, G.Ö., Koshland, D.E., and Greene, E.C. (2016). Single-molecule imaging reveals a collapsed conformational state for DNA-bound cohesin. Cell Rep. *15*, 988–998.

Sofueva, S., Yaffe, E., Chan, W.-C., Georgopoulou, D., Vietri Rudan, M., Mira-Bontenbal, H., Pollard, S.M., Schroth, G.P., Tanay, A., and Hadjur, S. (2013). Cohesin-mediated interactions organize chromosomal domain architecture. EMBO J. *32*, 3119–3129.

Symmons, O., Uslu, V.V., Tsujimura, T., Ruf, S., Nassari, S., Schwarzer, W., Ettwiller, L., and Spitz, F. (2014). Functional and topological characteristics of mammalian regulatory domains. Genome Res. *24*, 390–400.

Tedeschi, A., Wutz, G., Huet, S., Jaritz, M., Wuensche, A., Schirghuber, E., Davidson, I.F., Tang, W., Cisneros, D.A., Bhaskara, V., et al. (2013). Wapl is an essential regulator of chromatin structure and chromosome segregation. Nature *501*, 564–568.

Ulianov, S.V., Khrameeva, E.E., Gavrilov, A.A., Flyamer, I.M., Kos, P., Mikhaleva, E.A., Penin, A.A., Logacheva, M.D., Imakaev, M.V., Chertovich, A., et al. (2016). Active chromatin and transcription play a key role in chromosome partitioning into topologically associating domains. Genome Res. *26*, 70–84.

Van Bortle, K., Nichols, M.H., Li, L., Ong, C.-T., Takenaka, N., Qin, Z.S., and Corces, V.G. (2014). Insulator function and topological domain border strength scale with architectural protein occupancy. Genome Biol. *15*, R82.

Vietri Rudan, M., Barrington, C., Henderson, S., Ernst, C., Odom, D.T., Tanay, A., and Hadjur, S. (2015). Comparative Hi-C reveals that CTCF underlies evolution of chromosomal domain architecture. Cell Rep. *10*, 1297–1309.

Wang, X., Le, T.B.K., Lajoie, B.R., Dekker, J., Laub, M.T., and Rudner, D.Z. (2015). Condensin promotes the juxtaposition of DNA flanking its loading site in Bacillus subtilis. Genes Dev. *29*, 1661–1675.

Williamson, I., Berlivet, S., Eskeland, R., Boyle, S., Illingworth, R.S., Paquette, D., Dostie, J., and Bickmore, W.A. (2014). Spatial genome organization: contrasting views from chromosome conformation capture and fluorescence in situ hybridization. Genes Dev. *28*, 2778–2791.

Xiao, T., Wallace, J., and Felsenfeld, G. (2011). Specific sites in the C terminus of CTCF interact with the SA2 subunit of the cohesin complex and are required for cohesin-dependent insulation activity. Mol. Cell. Biol. *31*, 2174–2183.

Yaffe, E., and Tanay, A. (2011). Probabilistic modeling of Hi-C contact maps eliminates systematic biases to characterize global chromosomal architecture. Nat. Genet. *43*, 1059–1065.

Zuin, J., Dixon, J.R., van der Reijden, M.I.J., Ye, Z., Kolovos, P., Brouwer, R.W., van de Corput, M.P., van de Werken, H.J., Knoch, T.A., van IJcken, W.F., et al. (2014). Cohesin and CTCF differentially affect chromatin architecture and gene expression in human cells. Proc. Natl. Acad. Sci. USA *111*, 996–1001.